



KNN/PDMS/C-based lead-free piezoelectric composite film for flexible nanogenerator

Mengjie Xia¹ · Cuixian Luo¹ · Xiaoxiao Su¹ · Yinhui Li¹ · Pengwei Li¹ · Jie Hu¹ · Gang Li¹ · Huabei Jiang² · Wendong Zhang¹

Received: 13 January 2019 / Accepted: 4 March 2019 / Published online: 11 March 2019
© Springer Science+Business Media, LLC, part of Springer Nature 2019

Abstract

A novel approach to fabricate a high performance flexible piezoelectric nanogenerator (PNG) by employing $K_{0.5}Na_{0.5}NbO_3$ (KNN)/PDMS/C composite thin film has been proposed. The formed 12 wt% C doping KNN/PDMS PNG demonstrates a higher relative permittivity (ϵ_r , 173.56) and larger remanent polarization (P_r , $1.84 \mu\text{C}/\text{cm}^2$) than pure KNN/PDMS film, thus serving as the possible origins of their comparative piezoelectric activities, which could generate an maximum output voltage of 10.55 V (3.3 times as much as the PNG without C doping). Besides, the PNG is able to light up a commercial green light-emitting diode (LED) through an energy storage capacitor (47 μF), showing its great potential as power of wearable and mobile devices.

1 Introduction

Power generation using fossil energy resources now causes many problems as depletion of fossil energy and serious environmental pollution, piezoelectric nanogenerator (PNG) has gained much attention owing to develop sustainable and renewable energy generation technologies [1–5]. PNG shows superior advantages, it can convert the electricity from very accessible mechanical energy sources which exist widely in the environment. Due to its relatively small size, simple fabrication design, long cycle life, work steadily (relatively smaller influences from external conditions) and the environmentally friendly characteristic, piezoelectric power generation is a very promising approach to realize self-powering electronic devices. Piezoelectric materials such as ZnO [6, 7], lead zirconate titanate (PZT) [8, 9], lead

magnesium niobium titanate (PMNT) [10] and barium titanate (BTO) [11] have been widely investigate to fabricate the PNG. Despite advances in ZnO, low piezoelectric coefficient limits further improvement of the output performances. Besides, the lead element in PZT and PMNT is a serious threat to human health and environment although they have remarkable piezoelectric coefficient. Thus, lead-free BTO and $K_{0.5}Na_{0.5}NbO_3$ (KNN)-based materials have drawn significant attentions, especially KNN materials with high Curie temperature ($T_c \sim 420^\circ\text{C}$), good piezoelectric constant ($d_{33} \sim 160 \text{ pC/N}$) and biocompatibility (verified through cell culturing and live/dead cell staining of MC3T3) [12, 13]. Biocompatibility means that the PNG can play a critical role in biomedical applications [14].

However, pure KNN materials still turn out to be somewhat less effective in terms of the piezoelectric output compared with commercial lead piezoelectric materials; composition method has been used to further improve output energy [15, 16]. Recently, Wanget al [17]. reported single-crystalline KNN nanorods connected by interdigital Au/Ti electrodes on a flexible substrate, exhibited an open-circuit voltage (V_{oc}) of $\sim 30 \text{ mV}$. In order to improve the piezoelectric output of the materials and adapt to the new applications of flexible devices, piezoelectric materials and flexible polymer materials (such as PDMS or PVDF) are combined to obtain independent flexible composite piezoelectric materials and devices [18, 19]. Indeed, there is no good performance for the PNG based on pure piezoelectric

Electronic supplementary material The online version of this article (<https://doi.org/10.1007/s10854-019-01070-0>) contains supplementary material, which is available to authorized users.

✉ Pengwei Li
lipengwei@tyut.edu.cn

¹ Micro-Nano System Research Center, College of Information and Computer, Taiyuan University of Technology, Taiyuan 030024, Shanxi, China

² Biomedical Optics Laboratory, Department of Medical Engineering, College of Engineering, University of South Florida, Tampa, FL 33620, USA

materials or pure flexible polymer materials. TeKa et al. [20] reported pure PVDF-based nanogenerator could generate an output voltage of ~ 50 mV. Therefore, piezoelectric composite is a good choice for fabricating the PNG. Kang et al. [21] reported a PNG based on KNN nanoparticles (NPs) embedded in poly (vinylidene fluoride–trifluoroethylene) [P(VDF–TrFE)] polymer, an output voltage of ~ 0.98 V and an output current of ~ 78 nA were obtained for the nanofibers containing 10 vol% KNN. TeKa et al. [20] reported the PVDF/KNN nanocomposite—based nanogenerator could generate an output voltage of ~ 1.9 V. Moreover, Some one-dimensional structured materials such as CNT [22], Cu nanorods [23], and Ag NWs [24] used as fillers to synthesize composite with piezoelectric nanoparticles, the piezoelectric output of the PNG based on piezoelectric composite has significantly increased. However, the fundamental reasons of influencing the output performance of piezoelectric composite were not systematically studied in previous works. In addition, the non-uniform distribution of fillers or their aggregation into large clusters can decrease the effective surface area of fillers particles per unit volume, resulting in a lower relative permittivity [25]. Therefore, the content of piezoelectric particles and the choice of fillers, as well as their mass ratio will ultimately affect the output performance of the composite thin film.

Here, we reported a flexible PNG based on lead-free piezoelectric composite thin film obtained by dispersing KNN NPs and KNN/C in a PDMS matrix. KNN NPs were synthesized by a facile solid-state method, and the composite thin film was prepared by the spin-coating process. The effects of the concentrations of KNN and C on the output performance of the PNG were systematically investigated. The generating power stored in the capacitor can instantly light a commercial LED, indicated that this novel lead-free composite thin film might be an alternative candidate as a piezoelectric energy transformer. Besides, it is low-cost and facile fabrication, which has the potential for large-scale production of a high performance PNG.

2 Experimental

2.1 Synthesis of $K_{0.5}Na_{0.5}NbO_3$ (KNN) NPs

KNN NPs were synthesized using solid state reaction technique. K_2CO_3 (AR, 99.9%, Sinopharm Chemical Reagent Co., Ltd), Na_2CO_3 (AR, 99.9%, Beijing HuatengCo., Ltd), Nb_2O_5 (AR, 99.9%, Shanghai Macklin Biochemical Co., Ltd) were used as the raw materials. In a typical procedure, the original materials were weighed according to their stoichiometric ratio and ball-milled with absolute ethyl alcohol for 20 h on a planetary ball mill. The milled mixture was dried at 90°C for 6 h, and then calcined at different

temperatures (from 800 to 1000°C , temperature interval for 50°C) for 4 h.

2.2 Fabrication of KNN/PDMS/C-based PNG

In a typical procedure, the polydimethylsiloxane (PDMS; Sylgard 184, Dow Corning Corp., Auburn, MI) solution was prepared by adding curing agents to base (where weight ratio of PDMS and curing agent = 10:1), and then the synthesized KNN (30 wt%) and C (acetylene carbon black, 0, 3, 6, 9, 12, 15 wt%) were dispersed into the PDMS. Next, the mixture is spin-casted onto an Si wafer piece ($2.5\text{ cm} \times 2.5\text{ cm}$) with a spinning rate of 500 rpm for 45 s (obtain the film thickness of about $240\ \mu\text{m}$) and then cured in an oven at 90°C for 20 min. The cured composite thin film with KNN clusters was peeled off from the Si substrate. Then, the Cu electrode was both pasted to the top and the bottom surface of the composite film directly and fully cured. Further, the two electrodes were both pasted onto the PET substrate, the PET substrate served as a protective layer for the PNG device. And finally, the fabricated device was poled at 80°C while applying an electric field of 150 kV/cm for 12 h.

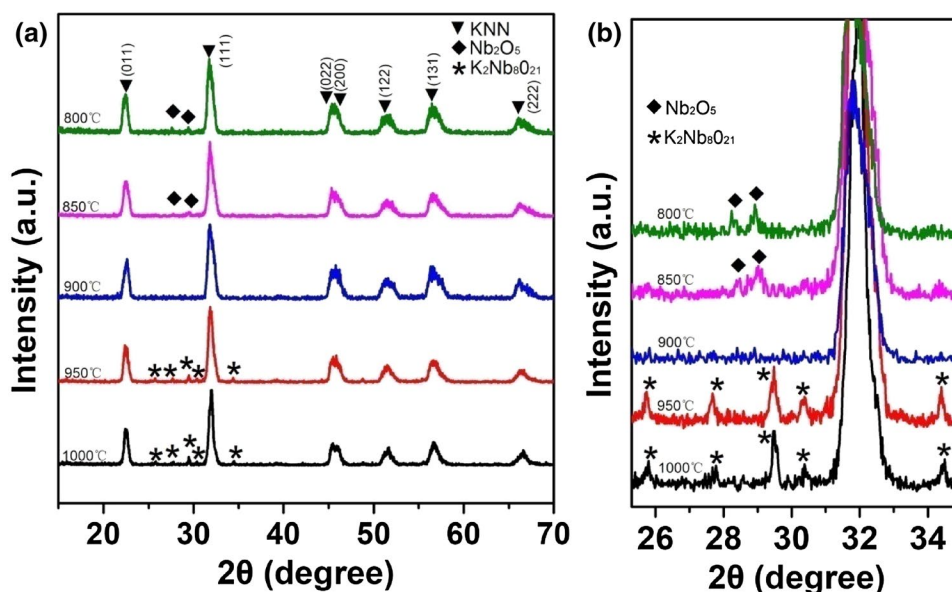
2.3 Characterization

The morphology and structure of the as-prepared KNN NPs were analyzed by using scanning electron microscopy (SEM, S-4800, Hitachi, Japan) and X-ray diffraction techniques (XRD, Rigaku Co., Tokyo, Japan). The dielectric properties of the composite thin films within the frequency range of 1 kHz–5 MHz were measured by using LCR tester (E4980AL, Agilent, USA) and the electric hysteresis loop was measured by ferroelectric analyzer (RTI-Multiferroic, Radiant, USA) with the frequency of 1 Hz at room temperature. The output voltage and current from the PNGs were measured by a digital oscilloscope (33522A, Agilent, USA) and a source measurement unit (2400 SMU, Keithley, USA), respectively. The beating for PNGs was provided by a shaker (ESS-025, Dongling vibration test instrument Co., Ltd., China).

3 Results and discussion

The purity and crystallinity of the typically synthesized KNN NPs were examined by XRD (Fig. 1). Three kinds of substances could be found in the XRD patterns, one was typical orthorhombic structure of KNN [26], and the others were indexed to orthorhombic Nb_2O_5 (JCPDS-ICDD file no. 71-0336) and $K_2Nb_8O_{21}$ (JCPDS-ICDD file no. 31-1060), respectively. When the calcined temperature changed from 800 to 1000°C (Fig. 1a), the pure phases KNN could only be acquired at the temperature of 900°C . On the one hand,

Fig. 1 **a** XRD pattern of KNN calcined at different temperatures, from 800 to 1000 °C, **b** the partial enlarged (with diffraction angle from 25 to 35°) XRD pattern of the prepared samples



if the calcined temperature was too low, impure phase of Nb_2O_5 crystal would appear in the final products. On the other hand, when the calcined temperature was too high, impure phase of $\text{K}_2\text{Nb}_8\text{O}_{21}$ crystal would appear in the final products (Fig. 1b). At lower temperature (800 °C and 850 °C), the two low-intensity extra peaks presented at 28.4° and 28.9°, show the traces of unreacted Nb_2O_5 , indicating the temperature was insufficient to activate Nb_2O_5 to react with alkali carbonates fully. At reaction temperature of 900 °C, single phase perovskite structure of KNN could be detected in XRD pattern, showing that all the raw materials were fully reacted in the solid-state reaction (1) of KNN synthesis. When the calcined temperature was higher than 950 °C, the secondary phase of $\text{K}_2\text{Nb}_8\text{O}_{21}$ could be found in XRD pattern. The reason of which may be explained by the higher melting point of K_2CO_3 (891 °C) than Na_2CO_3 (851 °C), this would lead to more loss of the Na element than K element with the reactions (2 and 3) proceeding [27], and finally resulted in the formation of $\text{K}_2\text{Nb}_8\text{O}_{21}$ in the KNN products (reaction 4).

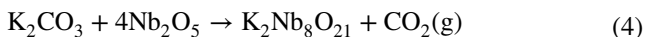
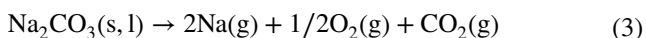
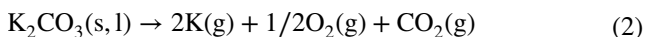
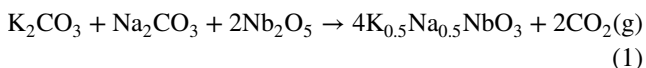


Figure 2a shows SEM image of KNN NPs calcined at 900 °C for 4 h, exhibiting the cubic shape with low agglomeration. The average particle size of KNN NPs is 280 ± 160 nm (Fig. 2b). Figure 2c shows the illustration for KNN of orthorhombic structure at room temperature, which

possesses monoclinic symmetry, with lattice parameters $a_m = c_m < b_m$, while b_m axis is perpendicular to $a_m c_m$ plane and angle β a little more than 90° [28]. Due to angle β is very close to 90°, b_m axis is not much bigger than a_m axis in length. Therefore, it can be considered as a cube structure approximatively, which can also explain the cuboidal morphology of KNN in Fig. 2a.

Schematic illustration of the process for fabricating the PNG is shown in Fig. 3a. The process contains four main steps including spin-coating, curing, peel-off and packaging, and detail information described in Sect. 2. Figure 3b shows the PNG bent by human fingers, confirming the suitability for use in flexible and embedded electronics.

After the poling at 80 °C under an electric field of 150 kV/cm for 12 h, the output performance of the PNGs based on KNN/PDMS composite thin film under the periodic beating from mechanical vibrator at a frequency of 10 Hz was measured in Fig. 4. The voltage (and the current) of the KNN/PDMS composite PNGs increases from 0.67 to 5.38 V (corresponding to the current from 0.07 to 0.62 μA), with the concentration of KNN NPs increasing from 10 to 40 wt% (Fig. 4a, b). It can be found that both the output voltage and current gradually increase with the content of KNN NPs, indicating the output performance of the PNG is dominated by KNN NPs. In addition, the output performance for different film thickness KNN/PDMS composite PNGs is shown in Fig. S1. Obviously, the output voltage increases with the thickness of the film, which can also be explained by the increase of the quantity of KNN NPs in unit area of the film.

In order to confirm the validity of the output electric signals, which were purely generated from the piezoelectric phenomenon of the PNG, linear superposition

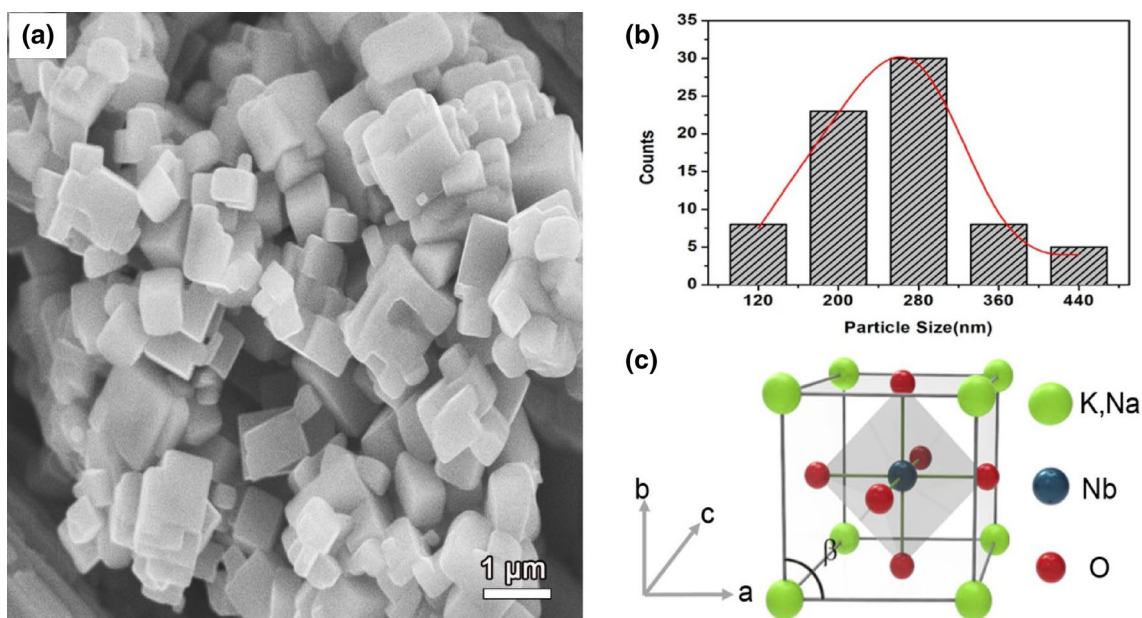
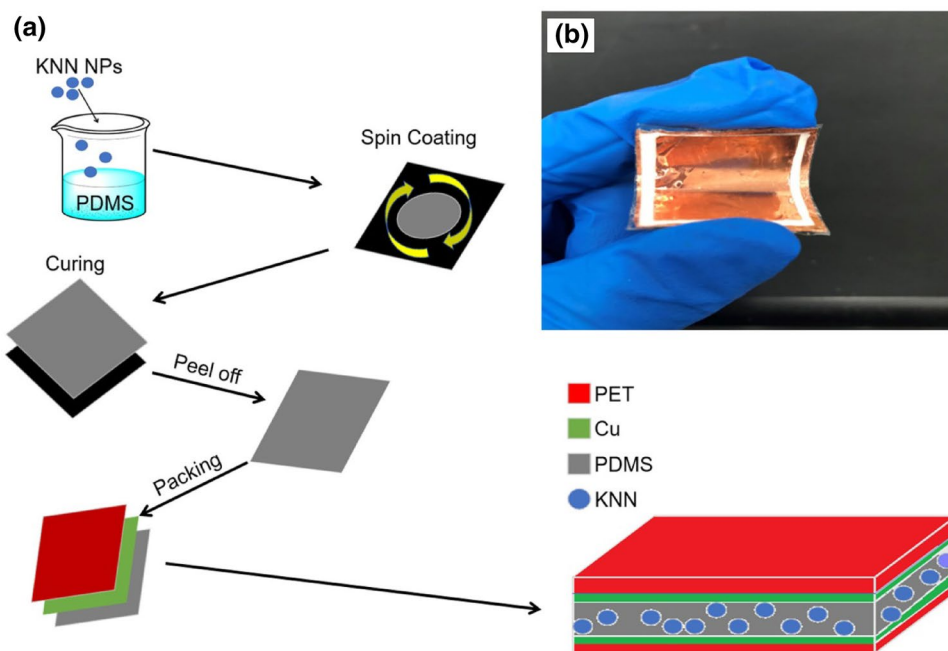


Fig. 2 The morphology and structure of KNN NPs. **a** SEM image, **b** size distribution, and **c** illustration of orthorhombic structure for KNN at room temperature

Fig. 3 a Schematic illustration of the process for fabricating the PNG. **b** Photograph of the real flexible PNG



tests and switching-polarity tests [29, 30] have been performed. Figure 4c shows the linear superposition tests of the PNGs with KNN concentration of 10 wt% and 20 wt%, respectively. The output voltage of the PNGs under the serial connection mode can reach up to 2.31 V, which is approximately equal to the output voltage superposition of two PNGs. Switching-polarity tests are shown in Fig. 4d, when the PNG (KNN concentration 30 wt%) is forward

connected to the measurement device, a positive voltage generated can be detected. While under reverse connection, an opposite output voltage signal is measured, whose amplitudes are almost the same as the one under forward connection. These results confirm that the detected output signals are indeed from the PNG. Taking into account several aspects like electrical output, craftsmanship and

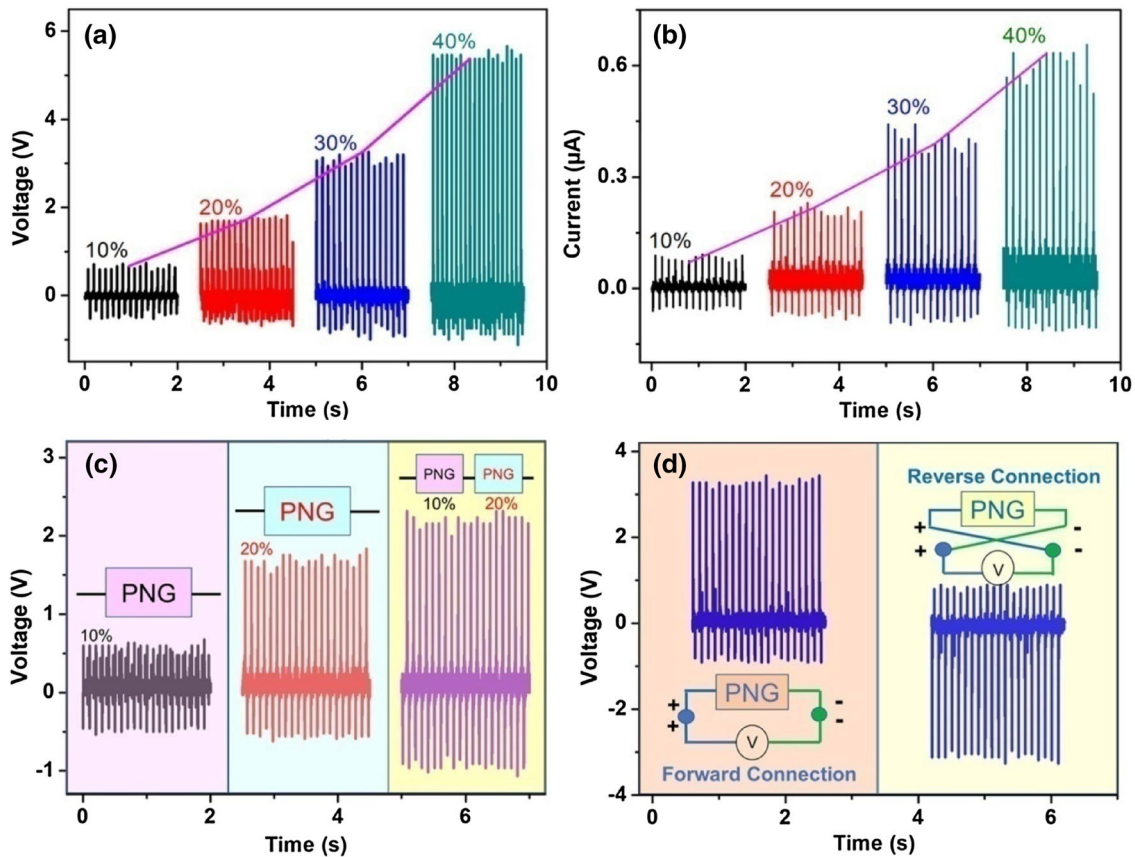


Fig. 4 The output performance of PNGs based on KNN/PDMS composite thin film. **a** Time-dependent output voltage for PNGs with 10, 20, 30 and 40 wt% KNN NPs concentration. **b** Time-dependent output current for PNGs with 10, 20, 30 and 40 wt% KNN NPs concen-

tration. **c** Open circuit voltage of the PNG (KNN NPs concentration 10 wt%) and the PNG (KNN NPs concentration 20 wt%) with series connection. **d** Open circuit voltage of the PNG (KNN NPs concentration 30 wt%) in the forward connection and reverse connection

flexibility, the film thickness of 240 μm and 30% KNN concentration have been chosen to make a compromise.

Based on percolation theory [31–33], carbon materials (like acetylene black, rGO, CNT, etc.) were usually employed as conductive phase in piezoelectric composites to improve the migration rate of the polarization charges. But carbon doping is rarely used in KNN material, in Park's [34] work, CNT is used for enhancement of voltage generation of piezoelectric devices with BaTiO₃ NPs. The CNT's role in the piezoelectric device as dispersant, stress reinforcing agent, and an conducting functional material. The content of CNT is controlled so that they do not affect the dielectric property of the entire structure. Thus, in this work, commercial acetylene black was selected as the carbon source, which was used as a filler to synthesize KNN/PDMS/C composite thin films with KNN NPs. C-content-dependent output performance of the synthesized KNN/PDMS/C-based composite thin film PNGs have been measured in Fig. 5. Output voltages around 3.22, 3.47, 5.81, 8.01, 10.55 and 6.57 V from PNGs for C fractions of 0, 3, 6, 9, 12 and 15 wt%, respectively, can be obtained (Fig. 5a). The maximum

voltage of 10.55 V can be obtained at the C-content of 12 wt%. Compared to the other works based on KNN materials, the output performance of our work improves obviously (Fig. 5 a, b; Table 1). This result can be explained by percolation theory. When C content is below the threshold (12%), there is synergy between the conductive property and piezoelectric property, the migration rate of the polarization charges improved, and finally resulted in the increasing of the PNG's output performance. On the contrary, if the C content exceeds the threshold, the leakage effect gets enhanced and the piezoelectric property will decrease [35].

To further explain the enhancement of the output performance of the KNN/PDMS/C-based composite PNGs, the relative permittivity (ϵ_r) and the remanent polarization (P_r) of the samples have been investigated (Fig. 4c, d and Table S1), the results of which show that, both the ϵ_r and P_r of the samples have similar trend as the output voltage with C content varying. The maximum ϵ_r of 173.56 (at 1 kHz) and P_r of 1.84 μC/cm² can also be obtained at the C content of 12 wt% (Table S1). The frequency dependence (1 kHz–5 MHz) of the relative permittivity and dielectric

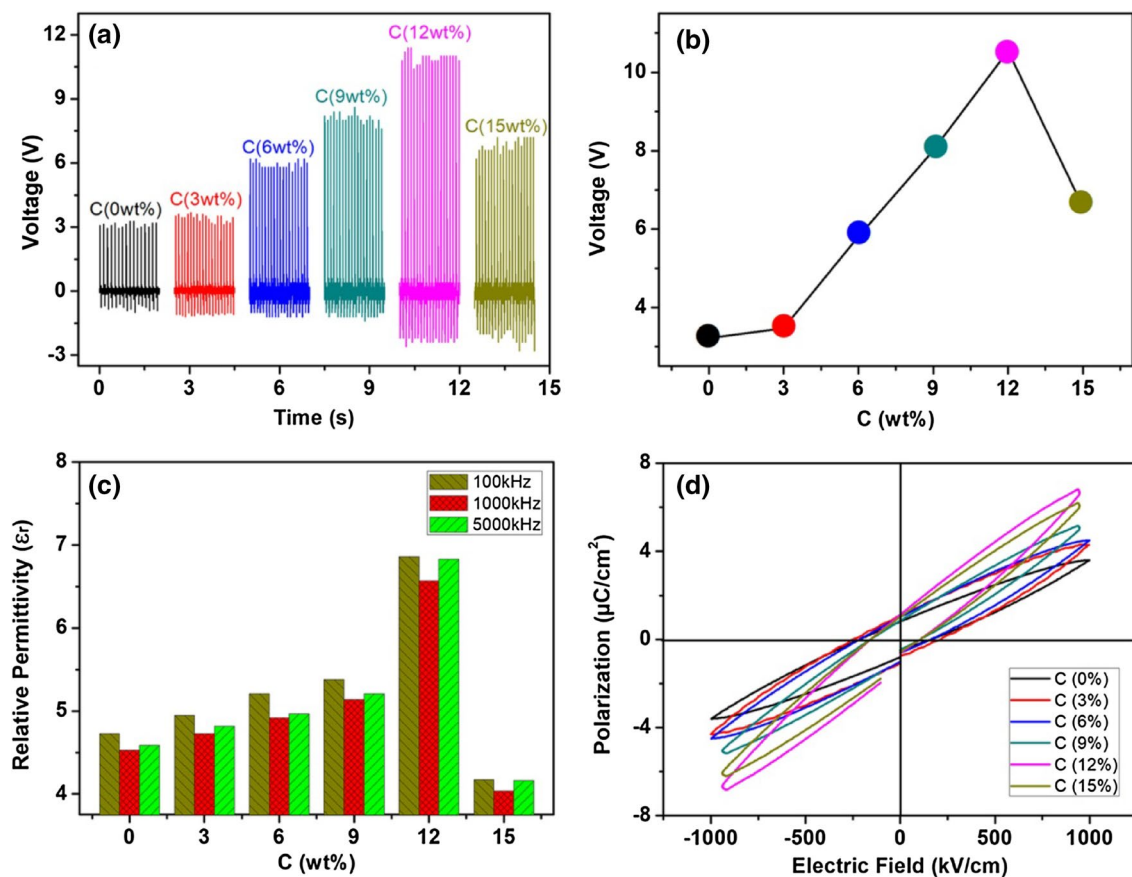


Fig. 5 **a** Time-dependent output voltage for of PNGs with different C content based on KNN/PDMS/C composite thin film. **b** The variation of open circuit voltage for PNGs with different C contents. **c** The relative permittivity of KNN/PDMS/C composite thin films with different

C content at different frequencies. **d** The polarization–electric field hysteresis loop of KNN/PDMS/C composite thin films with different C content

Table 1 Comparison of different piezoelectric nanogenerators

Active material	Form	Output	Ref.
PVDF	Pure PVDF nanoweb	50 mV	[20]
KNN	Nanorods	30 mV	[17]
KNN + PVDF	Composite	1.9 V	[20]
KNN + P(VDF–TrFE) nanofibers	Composite	0.98 V, 78 nA	[21]
PMN-PT + silicone rubber + CNT	Composite	4 V, 0.5 μA	[22]
KNN + PDMS	Composite	5.38 V, 0.62 μA	This work
KNN + PDMS + C	Composite	10.55 V	This work

loss ($\tan \delta$) of the composite films with different C contents at room temperature are shown in Fig. S2(a) and (b), they both perform the frequency dependence: ϵ_r and $\tan \delta$ decrease with increasing frequency. The relative permittivity drops fast at low frequency, then, decreases slowly and remains constant at high frequency. This may be attributed to space charge polarization [36, 37]. It is also observed that dielectric loss is quite smaller (0.10–0.12 at 1 kHz) compared to permittivity at any particular frequency, materials with high permittivity and low loss values have

more charge storage capability. It indicates that the composite films can be promising material for flexible charge storage device as well as other electronic devices [38]. The obtained P–E loop is shown in the Fig. 5d, it can be seen that the P_r of the composite film was first increased after C doping [Fig. S3(a)], the increase in P_r compared to KNN/PDMS film without C content doping, which suggests that the addition of C would enhance the ferroelectricity of the composite films. The reason of which may be explained by the change of domain structures of composite thin films

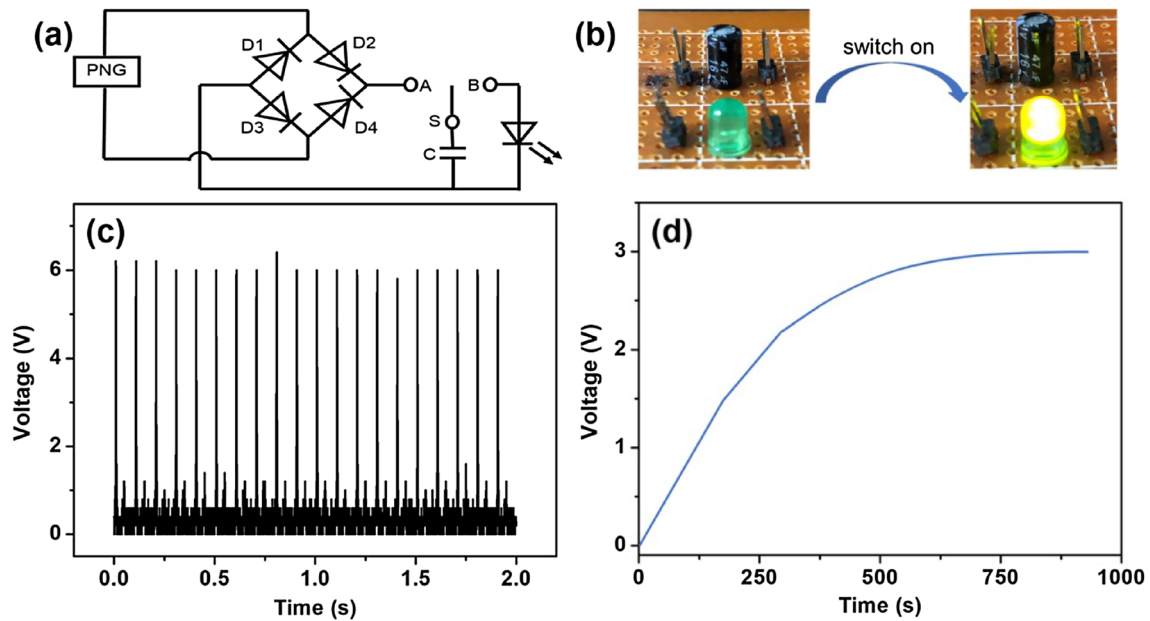


Fig. 6 **a** Circuit schematic of capacitor charging and LED driving. **b** The green LED was driven successfully, **c** rectified output voltage of the PNG. **d** The voltage of energy storage capacitor (47 μF) charging from the PNG by periodic beating

with different amounts of C doping [39]. When C content increases, the oxygen vacancy in the composite film is depressed and there is little domains are pinned. Thus, the ferroelectric polarization is enhanced [40]. The J–E curves are shown in Fig. S3(b), the leakage current density was first decreased then increased. One possible reason is that the addition of C content leads more homogeneous surface morphology, which is helpful to improve the leakage current property [41]. But when C content further increased to 12 wt%, the leakage current density started to increase. Similar results are seen in Co doping in KNN films, the possible reasons is that the excess Co ions might enter the interstice acted as new carriers or enter B-site led to the formation of new oxygen vacancies [42].

As known to all, the output performance of piezoelectric materials is closely related to their piezoelectric coefficients d_{33} , and the formula (5) is of great concern [43].

$$d_{33} = 2Q_{11}\epsilon_r\epsilon_0P_r \quad (5)$$

where $\epsilon_0 = 8.854 \times 10^{-12}$ F/m is the permittivity of vacuum, and Q_{11} (0.05–0.1 m^4/C^2) is the electrostrictive constant of the paraelectric phase. According to the formula and the experiment results (Fig. 5), Q_{11} and ϵ_0 are constant. This indicates that d_{33} is determined by the ϵ_r and P_r , which can also explain that why output voltage (Fig. 5a) of the samples show the similar variation trend with ϵ_r and P_r . In addition, it can be explained that the addition of acetylene black makes the free electron less prone to recombination in the composite material, resulting in a greater quantum yield of piezoelectric electrons [44, 45].

To verify the practicability of the practical application of the PNG, the KNN/PDMS/C-based composite PNG is connected with the energy storage capacitor (47 μF) and a commercial green LED through a bridge rectifier (converts the generated AC to DC signals), the schematic circuit diagram is displayed in Fig. 6a. When the control switch S is closed to the A, the rectified output power is charging the energy storage capacitor; while, if the switch was turn to B, the green LED is lit at once (Fig. 6b). Figure 6c shows the rectification output voltage of the PNG through bridge rectifier. And Fig. 6d shows the charging processes of the capacitor, where the saturated voltage of 3.02 V could be generated by the KNN/PDMS/C PNGs under repeated beating from mechanical vibrator after about 750 s. All of the above results indicate that the PNG can be used as a promising power source device for some tiny electronic devices. Moreover, to confirm mechanical reliable and endurance of the PNG, the durability test was conducted more than 4000 cycles. As shown in Fig. 7, it is observed that the generated output signals amplitude does not appear to change significantly even after 4000 cycles. This proves that the stability of the PNG, which is an important factor that makes the PNG very reliable for potential applications.

4 Conclusions

In summary, a high performance PNG by employing KNN/PDMS/C composite thin film has been demonstrated, which can generate high and steady electrical outputs. The electric

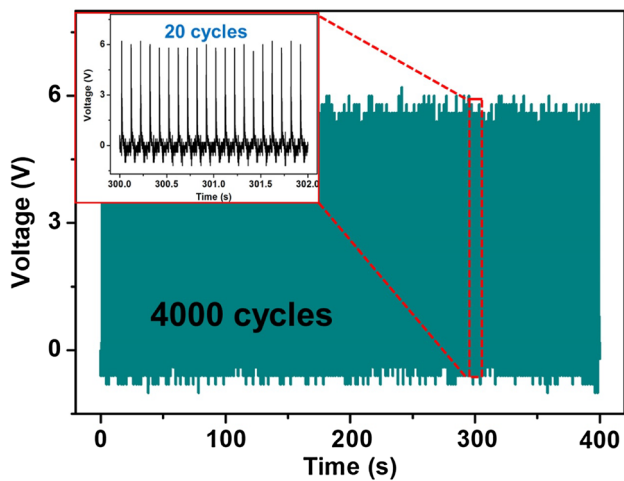


Fig. 7 The mechanical durability test of the PNG. Inset of which is partial enlarged signals from 300 to 302 s

output of the PNG based on KNN/PDMS/C composite thin films was systematically investigated with variation of the filling content of C (acetylene black), C plays a significant role in regulating the ϵ_r and P_r values of the composite thin film. When the content of C reaches threshold (12%), the ϵ_r and P_r reaches the maximum value of 173.56 (at 1 kHz) and $1.84 \mu\text{C}/\text{cm}^2$. Meanwhile, the output voltage of the PNG can reach up to 10.55 V, which is 3.3 times in comparison with KNN/PDMS PNG without C doping. The PNG can light up a commercial green LED through the energy storage capacitor, and its energy harvesting performance is durable and reliable energy. Our approach is simple and effective for fabricating low-cost, environmentally friendly, high performance, and stable mechanical energy harvesting devices.

Acknowledgements This work was supported by the Special Talents in Shanxi Province (Grant No. 201605D211020), the Projects of International Cooperation and Exchanges of Shanxi Province (Grant No. 201803D421029), and the Scientific and Technological Innovation Programs of Higher Education Institutions in Shanxi (Grant No. 2016136).

References

1. B. Sun, X. Li, R. Zhao, H. Ji, J. Qiu, N. Zhang, D. He, C. Wang, *J. Mater. Sci.* **54**, 2754 (2019)
2. E. Manolas, *Energy* **65**, 692 (2014)
3. Y. Liang, B. Yu, L. Wang, *Renew. Energy* **131**, 700 (2019)
4. E. Akrami, A. Gholami, M. Ameri, M. Zandi, *Energy Convers. Manage.* **175**, 21 (2018)
5. Z.L. Wang, W. Wu, *Angew. Chem. Int. Ed.* **51**, 2 (2012)
6. R. Yang, Y. Qin, L. Dai, Z.L. Wang, *Nat. Nanotechnol.* **4**, 34 (2009)
7. Q. Liao, Z. Zhang, X. Zhang, M. Mohr, Y. Zhang, H. Fecht, *Nano Res.* **7**, 917 (2014)
8. W. Wu, S. Bai, M. Yuan, Y. Qin, Z.L. Wang, T. Jing, *ACS Nano* **6**, 6231 (2012)

9. Q.L. Zhao, G.P. He, J.J. Di, W.L. Song, Z.L. Hou, P.P. Tan, D.W. Wang, M.S. Cao, *ACS Appl. Mater. Interfaces* **9**, 24696 (2017)
10. G.T. Hwang, H. Park, J.H. Lee, S. Oh, K.I. Park, M. Byun, H. Park, G. Ahn, C.K. Jeong, K. No, H. Kwon, S.G. Lee, B. Joung, K.J. Lee, *Adv. Mater.* **26**, 4880 (2014)
11. S.H. Shin, Y.H. Kim, M.H. Lee, J.Y. Jung, J. Nah, *ACS Nano* **8**, 2766 (2014)
12. Y. Guo, K.I. Kakimoto, H. Ohsato, *Appl. Phys. Lett.* **85**, 4121 (2004)
13. W. Chen, Z. Yu, J. Pang, P. Yu, G. Tan, C. Ning, *Materials* **10**, 345 (2017)
14. Y. Zhao, H. Fan, X. Ren, C. Long, G. Liu, Z. Liu, *J. Mater. Chem. C.* **4**, 7324 (2016)
15. G. Zhang, P. Zhao, X. Zhang, K. Han, T. Zhao, Y. Zhang, C.K. Jeong, S. Jiang, S. Zhang, Q. Wang, *Energy Environ. Sci.* **11**, 2046 (2018)
16. M. Shen, Y. Qin, Y. Zhang, M.A. Marwat, C. Zhang, W. Wang, M. Li, H. Zhang, G. Zhang, S. Jiang, *J. Am. Ceram. Soc.* (2019). <https://doi.org/10.1111/jace.16250>
17. Z. Wang, Y. Hu, W. Wang, D. Zhou, Y. Wang, H. Gu, *Integr. Ferroelectr.* **142**, 24 (2013)
18. X. Ren, H. Fan, Y. Zhao, Z. Liu, *ACS Appl. Mater. Inter.* **8**, 26190 (2016)
19. T. Huang, H. Yu, H. Wang, Q. Zhang, M. Zhu, *J. Phys. Chem. C* **120**, 26600 (2016)
20. A. Teka, S. Bairagi, M. Shahadat, M. Joshi, S.Z. Ahammad, S.W. Ali, *Polym. Adv. Technol.* **29**, 2537 (2018)
21. H.B. Kang, C.S. Han, J.C. Pyun, W.H. Ryu, C.Y. Kang, Y.S. Cho, *Compos. Sci. Technol.* **111**, 1 (2015)
22. C.K. Jeong, J. Lee, S. Han, J. Ryu, G.T. Hwang, D.Y. Park, J.H. Park, S.S. Lee, M. Byun, S.H. Ko, K.J. Lee, *Adv. Mater.* **27**, 2866 (2015)
23. C.K. Jeong, K.I. Park, J. Ryu, G.T. Hwang, K.J. Lee, *Adv. Funct. Mater.* **24**, 2620 (2014)
24. C. Baek, J.H. Yun, J.E. Wang, C.K. Jeong, K.J. Lee, K.I. Park, D.K. Kim, *Nanoscale* **8**, 17632 (2016)
25. Y. Jin, N. Xia, R.A. Gerhardt, *Nano Energy* **30**, 407 (2016)
26. C. Jiten, M. Rawat, A. Bhattacharya, K.C. Singh, *Mater. Res. Bull.* **90**, 162 (2017)
27. A.B. Haugen, F. Madaro, L.P. Bjørkeng, T. Grande, M.A. Einarsrud, *J. Eur. Ceram. Soc.* **35**, 1449 (2015)
28. K. Wang, J.F. Li, *Appl. Phys. Lett.* **91**, 135 (2007)
29. R. Yang, Y. Qin, C. Li, L. Dai, Z.L. Wang, *Appl. Phys. Lett.* **94**, 022905 (2009)
30. K.I. Park, S.B. Bae, S.H. Yang, H.I. Lee, K. Lee, S.J. Lee, *Nanoscale* **6**, 8962 (2014)
31. Z. Dang, Y. Shen, C.W. Nan, *Appl. Phys. Lett.* **81**, 4814 (2002)
32. Z. Dang, Y. Lin, C.W. Nan, *Adv. Mater.* **15**, 1625 (2003)
33. L. Zhang, K. Chen, S. Wang, S. Chen, S. Niu, Z. Wang, P. Du, *Mater. Lett.* **233**, 306 (2018)
34. K.I. Park, M. Lee, Y. Liu, S. Moon, G.T. Hwang, G. Zhu, J.E. Kim, S.O. Kim, D.K. Kim, Z.L. Wang, K.J. Lee, *Adv. Mater.* **24**, 2999 (2012)
35. C. Seoul, Y.T. Kim, C.K. Baek, *J. Polym. Sci. Pol. Phys.* **41**, 1572 (2003)
36. M.S. Khandekar, R.C. Kambale, J.Y. Patil, Y.D. Kolekar, S.S. Suryavanshi, *J. Alloys Compd.* **509**, 1861 (2011)
37. V. Manikandan, A. Vanitha, E.J. Kumar, J. Chandrasekaran, *J. Magn. Magn. Mater.* **432**, 477 (2017)
38. S. Nayak, D. Khastgir, *J. Appl. Polym. Sci.* <https://doi.org/10.1002/APP.47307> (2019)
39. Y.M. You, W.Q. Liao, D. Zhao, H.Y. Ye, Y. Zhang, Q. Zhou, X. Niu, J. Wang, P.F. Li, D.W. Fu, Z. Wang, S. Gao, K. Yang, J.M. Liu, J. Li, Y. Yan, Y. Yan, R.G. Xiong, *Science* **357**, 306 (2017)
40. Y. Sun, F. Guo, Q. Lu, S. Zhao, *Ceram. Int.* **44**, 13994 (2018)
41. W. Xing, Y. Ma, Y. Bai, S. Zhao, *Mater. Lett.* **161**, 216 (2015)

42. L. Wang, W. Ren, P. Shi, X. Wu, J. Alloys Compd. **608**, 202 (2014)
43. J.L. Zhang, P.F. Ji, Y.Q. Wu, X. Zhao, Y.Q. Tan, C.L. Wang, Appl. Phys. Lett. **104**, 222909 (2014)
44. S. Barrau, P. Demont, A. Peigney, C. Laurent, C. Lacabanne, Macromolecules **36**, 5187 (2003)
45. A.K. Jonscher, Nature **267**, 673 (1977)

Publisher's Note Springer Nature remains neutral with regard to jurisdictional claims in published maps and institutional affiliations.